JOURNAL OF MATERIALS SCIENCE 27 (1992) 4523–4530

Pulsed laser treatment of plasma-sprayed thermal barrier coatings: effect of pulse duration and energy input

I. SMUROV *, A. UGLOV, YU. KRIVONOGOV
Baikov Institute of Metallurgy, USSR Academy of Science, Leninsky Prospect 49, Moscow, Russia
S. STURLESE, C. BARTULI‡
Centro Sviluppo Materiali S.p.A., P.O. Box 10747, Roma EUR, Italy

Pulsed laser treatments of plasma-sprayed thermal barrier coatings can provide good corrosion resistance of protected components without impairing thermal fatigue resistance of the ceramic layers. Laser treatments are performed over a wide range of pulse durations and energy inputs, and their effects on microstructure, crystalline grain size and chemical composition of the remelted thin upper layer are investigated. Particular attention is given to macro and microcracking originating on the surface, gas bubble motion inside the melted layer and consequent surface crater formation. Density, shape, dimension and distribution of craters in the laser-irradiated zone are correlated with pulse duration and energy input of the laser beam. A numerical simulation of temperature distributions and heat phenomena originating in the ceramic coating during laser irradiation is presented, in order to explain the influence of laser characteristics on the quality of the coating surface.

1. Introduction

Plasma-sprayed thermal barrier coatings (TBCs) on turbine blade airfoils [1–5] are still in the research and development stage: in fact, due to the extremely severe operating conditions of these components, thermal shock resistance and protection against high-temperature erosion and corrosion are requested simultaneously [6, 7]. Unfortunately, microstructural features improving one property are detrimental to the other: open porosity [8] and vertical cracks, while increasing the compliance of the ceramic coating, and making it strain tolerant and more resistant to thermal fatigue [9, 10], are also a vehicle for aggressive gases, thus promoting oxidation of the bonding layer, and eventually leading to spalling [11, 12].

Laser treatments [13–19] have a great potential in this field: by carrying out a partial remelting of a strictly controlled thin layer of the coating, they can seal the ceramic material from aggressive gases [14], thus improving corrosion resistance, without impairing thermal fatigue [20].

In comparison with continuous lasers, pulsed lasers are characterized by a highly localized action, and by a very small energy input during the treatment, and these characteristics can significantly reduce undesirable side effects such as horizontal cracking of the top surface or small heat-affected zones.

In the present paper the effects of pulsed laser treatments of zirconia–ceria–yttria thermal barrier coatings are illustrated and discussed: thickness, microstructure, grain size and chemical composition of the modified layer, gas bubble emission and surface morphology are analysed and correlated with laser characteristics (pulse duration and energy input). The results of a numerical simulation of the temperature distributions originating inside the ceramic coating during laser treatment are also presented.

2. Materials and methods

Air plasma spraying was used to prepare thermal barrier coatings, consisting of a 150 μm thick NiCoCrAlY type bonding layer (METCO powder 461 NS) and a 450 μm thick ZrO_2–25% CeO_2–2.5% Y_2O_3 top coat (METCO powder 205 NS).

Surface modifications of ceramic coatings were induced by means of pulsed laser treatments, performed in a wide range of laser pulse durations, from 10^{-8}–10^{-3} s. In the 4×10^{-3}–3×10^{-5} s range, two types of solid-state YAG:Nd lasers (wavelength $\lambda = 1.06$ μm), having pulse energies up to 15 and 0.5 J, respectively (USSR trade-mark "Kvant 15" and "LTI-402"), were operated in free-running or normal regimes; in the 10^{-5}–10^{-6} s range, an electro-ioniza-

---

* *Present address*: Ecole Nationale d'Ingenieurs de Saint-Etienne, 58, rue Jean Parot, 42023 Saint-Etienne Cedex 2, France.

‡ *Present address*: Dipartimento di Studi di Chimica e Tecnologia delle Sostanze Biologicamente Attive, Università "La Sapienza", P. le A. Moro 5, 00185 Roma, Italy.

tional CO_2 laser ($\lambda = 10.6$ μm), having a pulse energy up to 1.5 J, was used; finally, in the 10^{-7}–10^{-8} s range the LTI-402 laser was operated in Q-switched regime, with a pulse energy of 0.1–0.3 J.

The pulse frequency, varying from 2–25 Hz, was selected in order to obtain an overlap coefficient K ($K = (s - a)/s$, where s is the spot diameter and a is the scanning step) of 0.25–0.50, for a scanning velocity of 3–20 mm s^{-1}.

Surface morphology and coating microstructure were investigated by means of optical and scanning electron microscopy, before and after laser modifications.

3. Results and discussion

3.1. Melted layer

During laser treatment of plasma-sprayed TBCs, a melted layer is formed on the coating surface: Fig. 1 shows the melted zone, almost completely densified, of a typical ceramic coating after the laser treatment.

The thickness of the modified layer depends upon laser pulse energy density (E/S, where E is the energy per pulse and S is the area of the laser spot) and upon pulse duration, τ, as illustrated in Fig. 2a and b. As an example, for $\tau = 5 \times 10^{-6}$ s and $E/S = 60$ J cm^{-2} the melted layer thickness is about 1–5 μm, and for $\tau = 4 \times 10^{-3}$ s and $E/S = 100$ J cm^{-2} it is about 30 μm. In both cases, the unmelted layer, facing the bond coat, remains porous, thus retaining its thermal insulating properties and thermal shock resistance [9].

On cooling from the ceramic melting point down to room temperature, the densified layer cracks [13–15, 17, 20].

Fig. 3 shows the surface morphology of the melted layer: macrocracks, with a width of 1–3 μm, and sometimes exceeding the thickness of the melted layer to a certain extent, are clearly visible (Fig. 3a); individual segments of the surface have irregular shapes (Fig. 3b), and their size is almost independent of the energetic characteristics of the laser beam, with slight variations as a function of τ; for example, for τ values of 4×10^{-3} s and 5×10^{-6} s, segment sizes are in the range 100–200 μm and 70–150 μm, respectively.

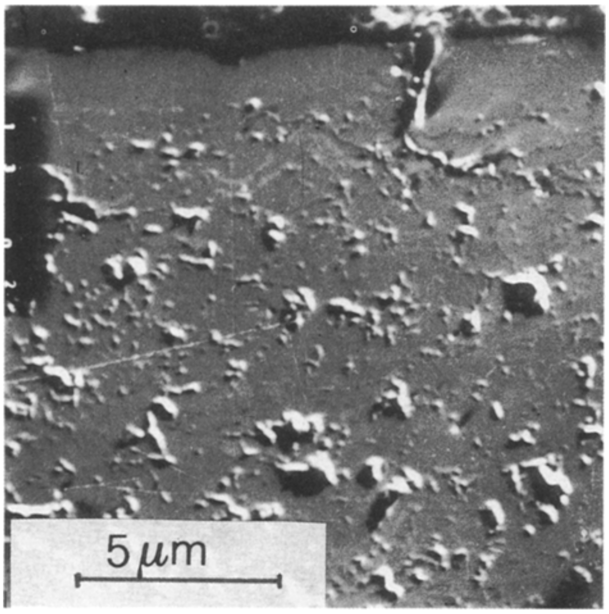

Figure 1 Cross section of a typical plasma-sprayed ceramic coating after laser treatment ($\tau = 4 \times 10^{-3}$ s, $E = 7$ J).

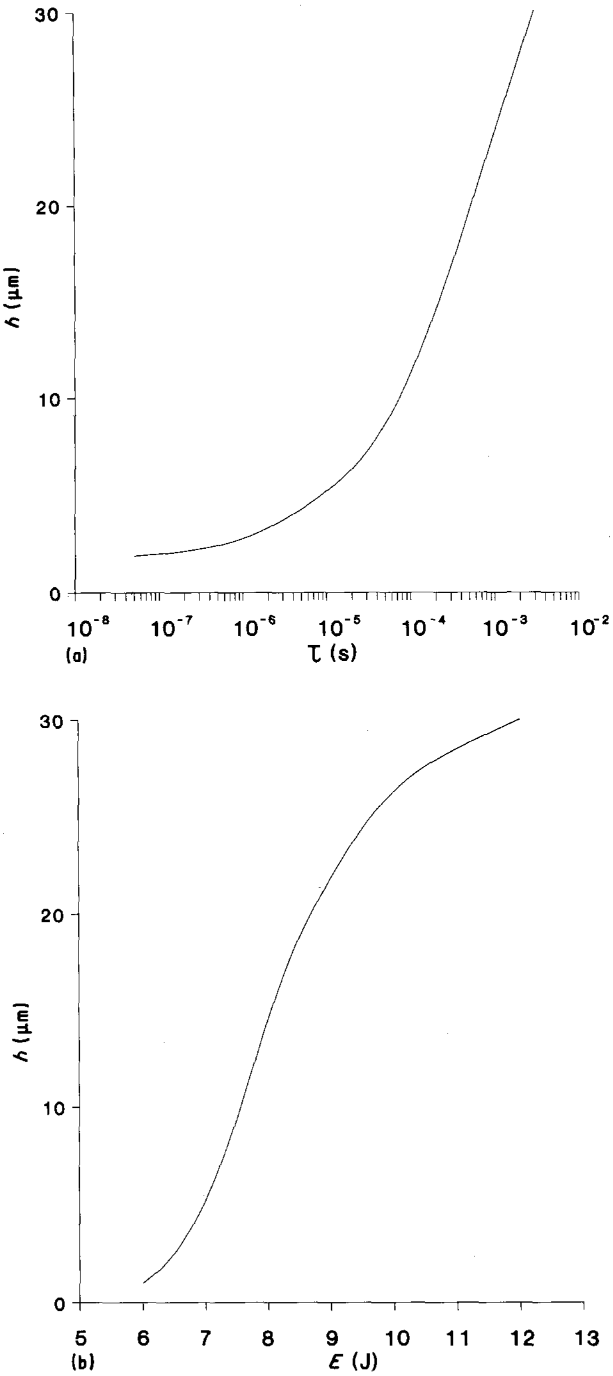

Figure 2 Melted layer thickness as a function of (a) laser pulse duration, t ($E/S = 80 \pm 20$ J cm^{-2}), (b) pulse energy input, E ($\tau = 4 \times 10^{-3}$ s).

Microcracks are also present on the melted surface beside macrocracks (Fig. 3c): they are characterized by many branches, having a length of a few micrometres and a width of some tens of a micrometre.

The presence of macro- and microcracks in the melted layer is a consequence of tensile stresses originating in the coating during cooling, when the modified

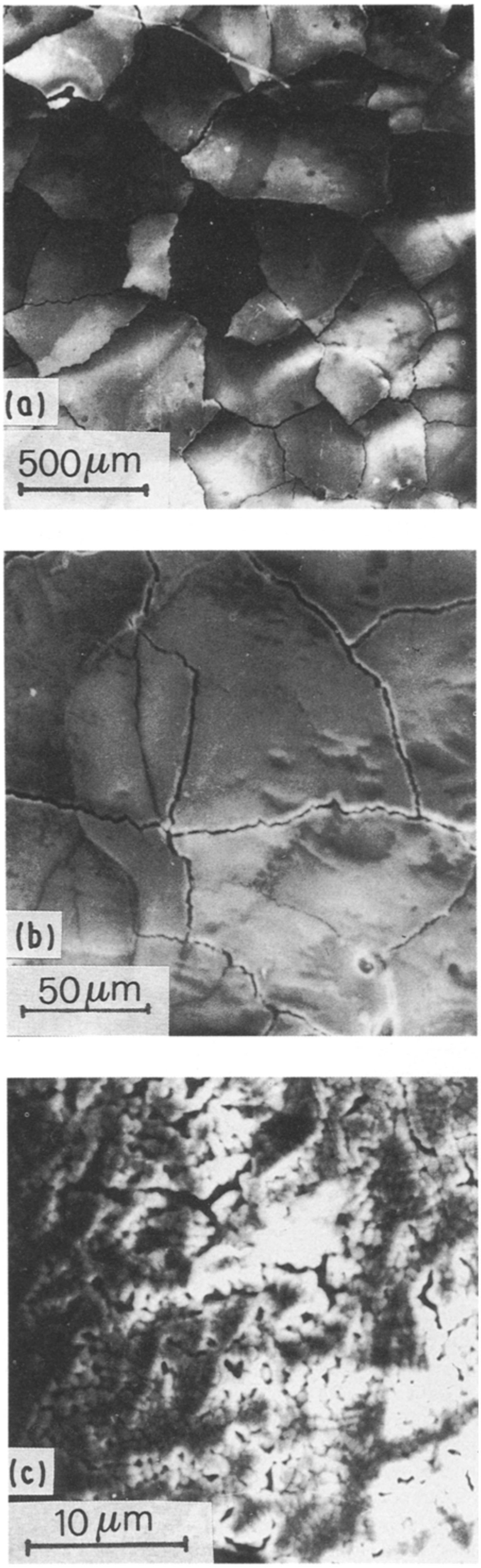

Figure 3 Surface morphology of the melted layer: (a) macrocracking pattern ($\tau = 4 \times 10^{-3}$ s, $E = E_{\mathrm{opt}}$), (b) individual segments ($\tau = 35 \times 10^{-6}$ s); (c) microcracks ($\tau = 4 \times 10^{-3}$ s, $E = E_{\mathrm{opt}}$).

upper zone of the coating, completely densified and almost free from porosity, tends to contract more than the unmelted and still porous layer. Moreover, residual pores, possibly entangled in the modified layer, can act as stress risers when the structure stiffens.

Another significant modification of the microstructure of the ceramic coating induced by laser treatment involves the crystalline grain size: in fact, recrystallization of the zirconia upper layer during the cooling stage of laser treatment is very rapid, leading to a fine grain structure. Grain size mostly depends on pulse duration: for a constant value of the energy flow ($q = 5 \times 10^4\ \mathrm{W\,cm^{-2}}$), the grain size is about 1–2 μm for a pulse duration value of 4×10^{-3} s, while a submicrometre grain structure is formed when τ decreases down to 5×10^{-6} s.

Finally, all laser treatments are characterized by a colour change of the melted layer, which implies a modification of its chemical composition. A convincing interpretation of this phenomenon is that a zirconium dioxide thermal dissociation of extremely thin layers (1–2 μm at $\tau = 1\text{–}1.5 \times 10^{-3}$ s and less than 0.3 μm at $\tau = 2\text{–}4 \times 10^{-6}$ s [21]) takes place during laser irradiation, leading to the formation of lower oxides of the ZrO_{2-x} type [21]. The reduced layer is extremely thin, and its thickness depends on pulse duration, being in the range 1–2 μm at $\tau = 1\text{–}1.5 \times 10^{-3}$ s, and decreasing to 0.3 μm at $\tau = 2\text{–}4 \times 10^{-6}$ s.

3.2. Gas emission

Morphology and structure analyses of the modified layer clearly demonstrate that its densification takes place under intensive gas emission conditions [20]. This phenomenon is mostly due to the release of inner gases entangled inside the pores or the cracks of the ceramic material, or physically and chemically adsorbed into the coating during the spraying process. Moreover, partial evaporation of the ceramic material must also be taken into account, due to the high temperatures attained during laser treatment.

The amount of residual porosity results from the competition of two factors: the velocity of gas bubble rise, and the dynamics of the melting (or solidification) front motion.

Gas bubble rising is strongly affected by surface tension gradient which, in turn, is an effect of the temperature gradient originating in the melted layer owing to the high energy density flux absorbed on the surface and to the low heat-transfer coefficient of the ceramic material.

In the experimental conditions described above (pulsed laser action, pulse duration $\tau \simeq 1$ ms, energy density flow $q \simeq 10^5\ \mathrm{W\,cm^{-2}}$), the influence of buoyancy force and convective mass transfer on bubble movement is small, compared with surface tension drift.

Gas bubble velocity, U, caused by surface tension drift is defined by the following equation [22]

$$U = \frac{1}{3}\left[\frac{R(\partial\sigma/\partial T)|\nabla T|}{\rho\nu}\right] \tag{1}$$

where R is the bubble radius, σ and ν are surface tension and kinematic viscosity of the melted material, respectively, ρ is its density, and $|\nabla T|$ is the temperature gradient in the liquid.

Equation 1 is derived assuming a steady state movement of a spherical bubble through a layer of infinite thickness, with constant temperature gradient [22]. Under these conditions, the bubble moves with a constant velocity, U, in the direction of temperature increase (in the present case, towards the irradiated surface of the melt).

Gas bubble rise in the melt, produced by the pulsed laser action, can be divided into two stages. The first stage takes place during laser irradiation, when the melting front moves downwards into the material; during this stage the temperature distribution along the axis perpendicular to the material surface is almost linear; as a consequence, the temperature gradient is almost constant and it is mainly determined by the absorbed energy density flow and by heat-transfer properties of the material [23]

$$\nabla T \simeq \frac{Aq}{h} \tag{2}$$

where q is the energy density flow, A is the material absorption capacity, and h the heat conductivity of the melt. At this stage, gas bubbles produced at the melting front rise to the surface under the action of the surface tension force gradient.

The shape of a gas bubble is defined by the (spheroidization time)/(bubble lifetime) ratio. As a first approximation, the spheroidization time, t_S, can be estimated as [21]

$$t_S = \frac{2R\rho\nu}{\sigma} \tag{3}$$

Usually $t_S \simeq 10^{-6}$–10^{-7} s. The bubble lifetime is determined by the velocity of bubble rise and by the thickness of the melt.

The lifetime of the ceramic material at the liquid state is indicated by t_l (melted layer lifetime); it has been demonstrated [24] that, under pulsed laser processing conditions, the value of t_l near the surface, which decreases as the distance from the surface increases, never exceeds twice the duration of the pulse. For pulse duration values up to 10^{-6} s, the condition

$$t_l > t_s \tag{4}$$

is valid all along the melted zone, with the exception of the narrow, deepest layer of the melt: this is the reason why the spheroidization of gas bubbles can take place.

In the second stage, immediately after the laser pulse termination, the melting front keeps moving down into the material for a certain time, due to the high melt overheating [24]. Therefore, new gas bubbles keep forming at the bottom of the melted layer.

However, after a sharp decrease in the temperature of the melt, caused in the surface layer by heat losses from the surface and heat removal from the bulk material, the solidification of the melted layer takes place at a temperature gradient very near to zero. As a consequence, the surface tension drift of gas bubbles practically stops at this stage: gas bubble motion to the surface is much slower, and rising velocity, v, under the action of the buoyancy force is approximately calculated as [21]

$$v \simeq \left(\frac{1}{3}\right)\left(\frac{gR^2}{\nu}\right) \tag{5}$$

where g represents the acceleration due to gravity.

First estimations show that the time necessary for a gas bubble to rise under the action of buoyancy force from a depth of 30 μm (which is a typical melted layer depth for a pulse duration of 4×10^{-3} s) is of the order of 10^{-3} s: therefore gas bubbles produced in the deepest zones of the melted layer do not have enough time to reach the surface during the melt lifetime. As a consequence, the production of residual porosity in the remelted layer is mainly determined by the bubbles produced during the final stage of laser irradiation, or just after its termination.

From the above discussion it is evident that gas emission dynamics is significantly affected by both laser pulse duration and energy, because these parameters define the melting and solidification front motion and have a great influence on the surface tension drift velocity.

3.3. Surface craters

As a result of laser treatment of porous coatings, typically many craters are observed on the irradiated surface. When the gas bubbles produced in the last stage of laser pulsing rise to the coating surface, the viscosity of the melted layer, on its way to solidifying, is very high. Sometimes, bubbles can be too slow to complete their rise before the ceramic material solidification, so that a sort of sink, or crater, can remain on the top surface of the coating at the end of the laser treatment. Fig. 4 shows typical surface craters. Under the above conditions, the shape and the size of these craters, as well as their density, depend upon laser pulse characteristics.

Fig. 5 illustrates the dependence of crater density, d (number of craters measured per mm^2), upon pulse energy, E, for a constant value of pulse duration ($\tau = 4 \times 10^{-3}$ s). According to these results, an optimum range of pulse energy, corresponding to the minimal density of craters, can be identified: under these conditions, the surface of the melted layer is quite uniform, and the medium roughness of the ceramic coating decreases from 8–12 μm, measured before laser treatment, to about 1 μm. Best results were obtained for τ values of about 10^{-3} s and for the E_{opt} value of about 10 J. If laser treatments are performed out of the optimum energy range, a high crater density is observed, and surface quality is impaired. It has to be remembered that surface morphology plays a very important role on aerodynamic properties and thermal shock resistance of ceramic-coated turbine blades: in fact, surface roughness, acting as a stress riser, can lead to highly localized stress distributions, responsible for spalling and delamination of the coating. In order to avoid critical stress concentrations, crater density must be reduced to a minimum, thus

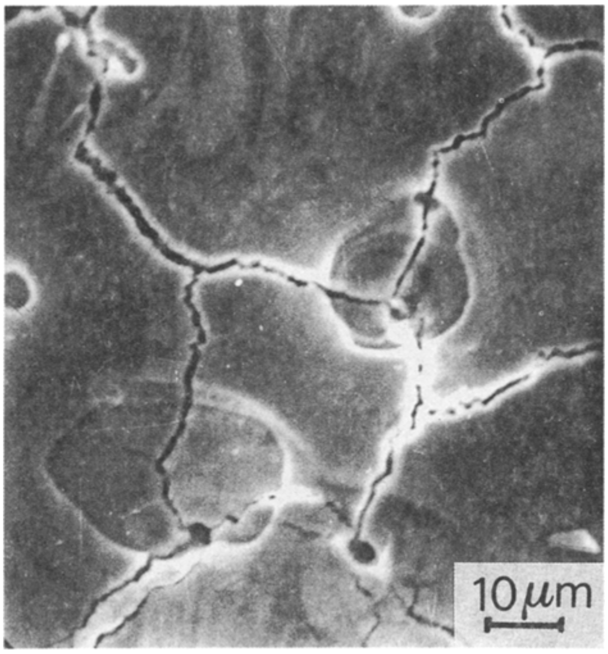

Figure 4 Typical craters originating on the surface of the coating ($\tau = 5 \times 10^{-3}$ s, $E/S = 30$ J cm^{-2}).

obtaining a smooth and dense surface of the ceramic layer.

In Fig. 6, the density, d, and the average diameter, D, of the craters are correlated with pulse duration, τ.

Crater size distribution, $\Delta N(D)/N$, is illustrated in Fig. 7: for $\tau = 4 \times 10^{-3}$ s, (Fig. 7a), crater diameters are distributed over a wide range, from just several micrometres to about 100 μm; on the contrary, experiments carried out with the pulse periodic electro-ionizational CO_2 laser demonstrate that for $\tau = 5 \times 10^{-6}$ s, (see Fig. 7b), crater size distribution is narrow, and the average diameter is about 2–3 μm. This is a consequence of the lower values of t_l, preventing gas bubbles from coalescing before rising. It has to be remarked that the mean crater size can be noticeably larger than the bubble diameter, due to wave propagation on the surface of the melt.

Finally, spatial distribution of surface craters was determined by both laser-beam spatial distribution and laser pulse energy: as clearly seen in Fig. 5, both increasing and decreasing the energy input from the optimal value (corresponding to the minimum value of surface craters), leads to an increase in crater density. This is the reason why in the case of non-uniform energy spatial distribution, a corresponding non-uniform crater distribution has to be expected. Craters distribution around the laser spot, $\Delta N(r)/N$ (where r is the distance from the axis of the laser beam) is represented in Fig. 8: the density of the craters originating within the laser spot area is minimal in the spot centre, and it sharply increases as r increases. In fact, according to the Gaussian spatial distribution of the energy in the laser beam, the highest values of temperature gradient inside the melt are localized in the centre of the laser spot; therefore, in that zone gas bubble surface tension drift velocity is maximum, thus reducing the density of residual craters to a minimum.

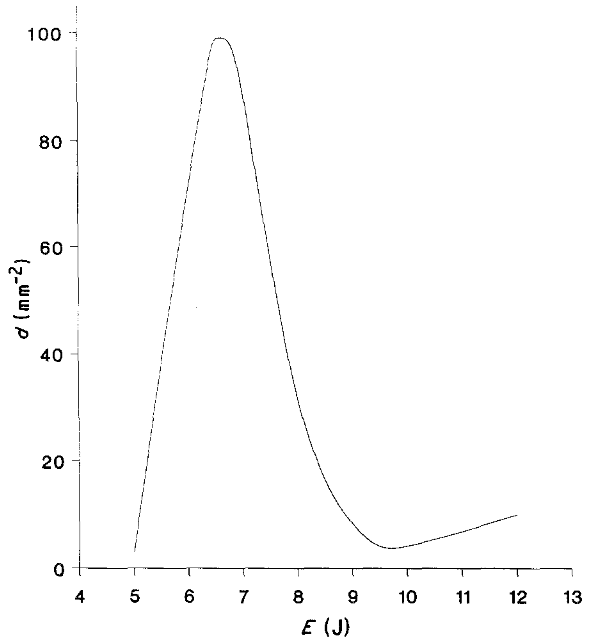

Figure 5 Effect of energy input on the density of surface craters ($\tau = 4 \times 10^{-3}$ s).

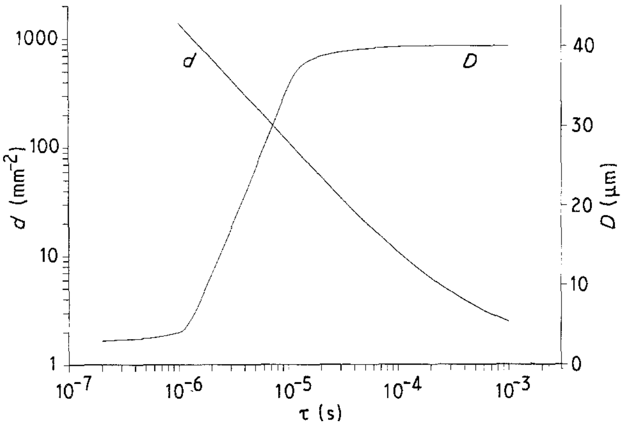

Figure 6 Effect of pulse duration on the average diameter, D, and on the density, d, of the craters ($E/S = 80$ J cm^{-2}).

3.4. Numerical simulation of heat phenomena

In order to explain and to predict the effect of laser characteristics on the quality of the laser-treated plasma-sprayed coatings, a numerical simulation of the temperature fields originating during the laser treatment was undertaken.

The mathematical model used to solve this problem has been largely described previously [24, 25]: it takes into account the processes of heating, melting, evaporation, solidification and cooling. As a first approximation, heat transfer was considered as a one-dimensional phenomenon.

The absorption capacity value used in the calculations was chosen to be equal to the original absorbance value, measured before the laser action by means of a reflectometric method: surface absorbance, A, was found to be 0.75.

As a result of the numerical simulations, time dependences of coating surface temperature over melting temperature ratio, T_s/T_m, melting and evaporation

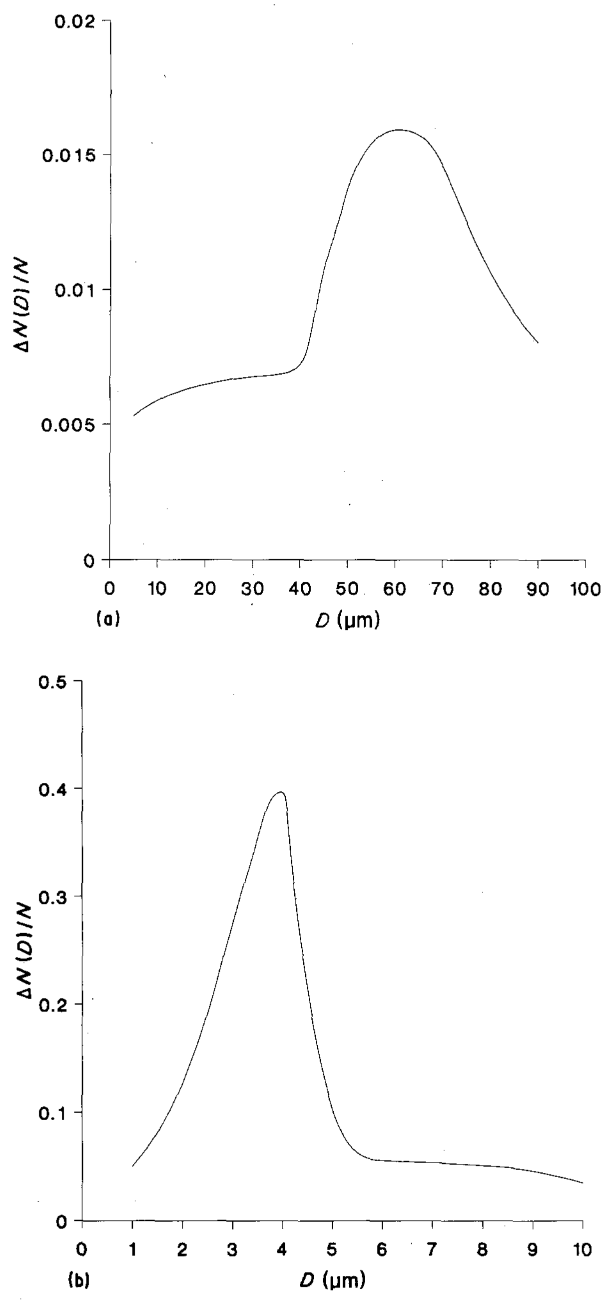

Figure 7 Size distribution of surface craters: $N(D)$ is the number of craters having a diameter D. (a) $\tau = 4 \times 10^{-3}$ s, (b) $\tau = 5 \times 10^{-6}$ s.

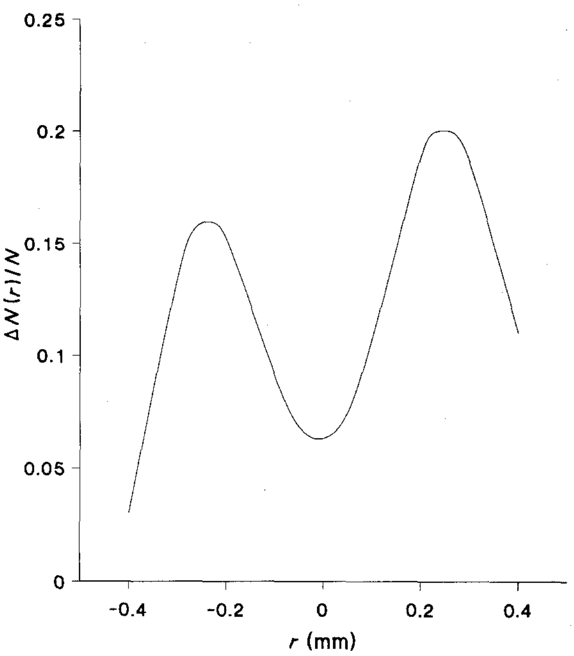

Figure 8 Distribution of craters inside the laser-irradiated zone: $N(r)$ is the number of craters situated at a distance r from the centre of the laser beam.

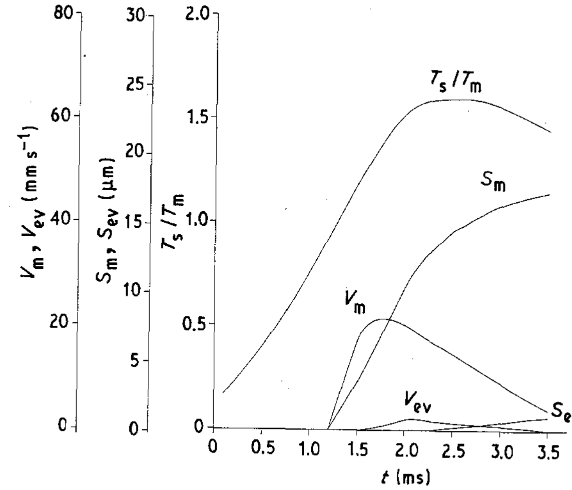

Figure 9 Time dependence of surface temperature/melting temperature, T_s/T_m, distance of the melting front, S_m, and the evaporation front, S_{ev}, from the original surface of the melt, melting front velocity, V_m, and evaporation front velocity, V_{ev} ($\tau = 4 \times 10^{-3}$ s, $E = E_{opt}$).

front distances from the original surface of the coating, S_m and S_{ev}, and phase front velocities, V_m and V_{ev}, are presented in Fig. 9, for the optimum value of the laser energy. It is evident that most of the upper layer modification occurs in a very strong overheating condition, determined by the low heat-transfer coefficient of plasma-sprayed zirconia [26]. Fig. 9 shows that the maximum temperature reached by the coating surface during laser action is about 4600 K ($T_s/T_m = 1.6$), and the melted layer depth at that time is 14 μm. The maximum value of the melt depth is achieved after the end of the laser pulse, and reaches 20 μm; this value agrees with experimental results with a 20% accuracy. In the upper zone of the melted layer, the temperature–depth dependence is linear, and the temperature gradient is about 1.2×10^8 K m^{-1}.

Fig. 10 illustrates the temperature distribution inside the coating at different moments of laser-beam processing, in the same energetic conditions. Calculations were made taking into account the real shape of the laser pulse.

In Fig. 11 the maximum temperature attained by the coating surface is correlated with laser-beam energy: after a linear increase of T_s^{max}/T_m, the maximum temperature reaches a plateau, and for $E > 1.4\ E_{opt}$ it remains almost constant. A similar plateau is observed also in the case of the T_s time dependence (see Fig. 9). In fact, when E exceeds a threshold value, T_s approaches the boiling point of the ceramic material (4900 K): as a consequence, evaporation is strongly enhanced, and the energy consumption is intensified.

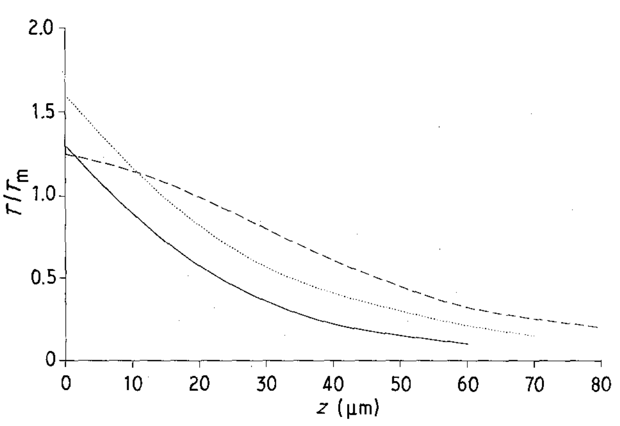

Figure 10 Temperature distribution inside the coating, at three different times ($E = E_{opt}$). t: (—) 1.8 ms, (. . .) 2.5 ms, (– – –) 4.0 ms.

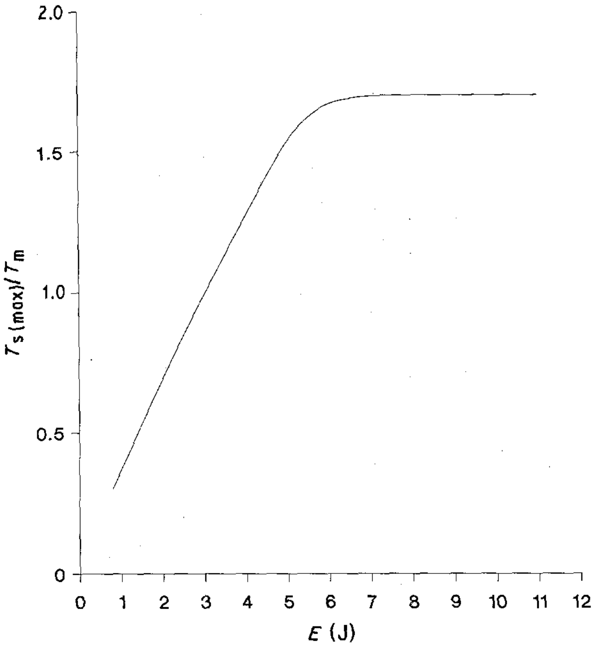

Figure 11 Maximum surface temperature as a function of the pulse energy input ($\tau = 4 \times 10^{-3}$ s).

On the basis of the temperature-field simulation, the crater density dependence from pulse energy, illustrated in Fig. 5, can be interpreted as follows: for a low energy input ($E \ll E_{opt}$), gas bubbles, produced during the liquid phase lifetime, coalesce and start moving towards the surface, but, due to the very short melted layer lifetime, they cannot leave the melt, thus forming a large number of craters (d reaches the maximum value). At $E \simeq E_{opt}$, the melted layer lifetime increases, reaching 3–4 × 10^{-3} s, and this time is sufficient for the gas emission process to be fully completed. As a result, crater density is minimal, and a smooth surface is formed. For $E > E_{opt}$, the temperature plateau is approached, and the process of extensive evaporation begins. Owing to the presence of a greater number of evaporation nuclei, the evaporation seems to be of a bulk type [27]: as a consequence, the number of craters is strongly increased, thus impairing the surface quality.

4. Conclusions

Pulsed laser treatments of plasma-sprayed zirconia–ceria–yttria thermal barrier coatings were performed for a wide range of pulse durations and energy inputs.

1. Macro and microcracking originate on the top surface of the coating as a consequence of the differential tensile stresses originating within the densified upper layer and the unmelted, porous layer, during the cooling stage.
2. Crystalline grain size was found to be very fine and homogeneous after laser treatment: the longer the duration of the laser pulse the higher the grain size.
3. Chemical composition of the modified upper layer was also investigated: a thermal dissociation of zirconium dioxide was observed, leading to the formation of ZrO_{2-x} type oxides.
4. Residual porosity was interpreted as a result of the competition of two processes: the rising of gas bubbles emitted during laser treatment into the melted layer, and the melting front motion.
5. Density, shape, dimensions and distribution of surface craters originating in the laser-irradiated zone were correlated with laser pulse duration and energy input: an optimum value of laser energy input has been established in order to minimize the density of the craters.

A numerical simulation of the temperature fields produced in the ceramic coating during laser irradiation was also presented and compared to experimental results. On the basis of the indications coming from these analyses, a first evaluation of the optimum processing conditions for laser treatment of zirconia–ceria–yttria thermal barrier coatings can be attempted: the optimum pulse duration, the best energy input and the most convenient laser scanning step can be chosen in order to guarantee good surface quality of the coatings, together with acceptable thermal properties and spalling resistance.

References

1. W. J. BRINDLEY and R. A. MILLER, *Adv. Mater. Proc.* **8** (1989) 29.
2. J. W. FAIRBANKS and R. J. HECHT, *Mater. Sci. Engng* **88** (1987) 321.
3. T. N. RHYS-JONES and F. C. TORIZ, *High Temp. Tech.* **7** (2) (1989) 73.
4. M. H. VAN DE VOORDE, M. G. HOCKING and V. VASANTASREE, *High Temp. Mater. Proc.* **7** (2–3) (1986) 107.
5. A. S. GROT and J. K. MARTYN, *Ceram. Bull.* **60** (8) (1981) 807.
6. B. C. WU, E. CHANG, S. F. CHANG and D. TU, *J. Amer. Ceram. Soc.* **72** (2) (1989) 212.
7. A. BENNET, *Mater. Sci. Tech.* **2** (1986) 257.
8. J. H. ZAAT, *Ann. Rev. Mater. Sci.* **13** (1983) 9.
9. S. STURLESE, R. DAL MASCHIO, C. BARTULI, N. ZACCHETTI and M. BERARDO, in "High Performance Films and Coatings", edited by P. Vincenzini (Elsevier Science, B.V., 1991) p. 353.
10. K. D. SHEFFLER, R. A. GRAZIANI and G. C. SINKO, NASA CR-167964 (1982).
11. R. A. MILLER and C. E. LOWELL, *Thin Solid Films* **95** (1982) 265.
12. R. SIVAKUMAR and M. P. SRIVATAVA, *Oxid. Metals.* **20** (3–4) (1983) 67.

13. F. S. GALASSO and V. VETTRY, *Ceram. Bull* **62** (2) (1983) 253.
14. I. ZAPLATINSKY, *Thin Solid Films* **95** (3) (1982) 275.
15. T. ARAHARI, T. SUZUKI, N. IWAMOTO, N. UMESAKI, *Adv. Ceram.* **24A** (1988) 549.
16. A. ADAMSKI and R. McPHERSON, in "Advances in Thermal Spraying" (Pergamon, Oxford, 1986), p. 555.
17. M. HAVRDA, K. VOLENIK, J. WAGNER and P. MRAZ, *ibid.*, p. 569.
18. N. IWAMOTO, N. UMESAKI and S. ENDO, *ibid.* p. 563.
19. R. A. MILLER and C. C. BERNDT, *Thin Solid Films* **119** (1984) 195.
20. R. SIVAKUMAR and B. L. MORDIKE, *Surf. Engng* **4** (2) (1988) 127.
21. A. A. UGLOV, V. A. GREBENNIKOV, I. YU. SMUROV and V. G. PANAETOV, *Phis. Khim. Obratotki Mater.* **3** (1988) 125.
22. A. A. UGLOV, I. YU. SMUROV, A. M. LASHIN and A. G. GUSKOV, "Heat processes of pulse laser treatments of metals" (Nauka, Moskow) in press.
23. N. RYKALIN, A. UGLOV, I. ZUEV and A. KOKORA, "Laser and electron beam materials processing" (Mir, Moscow, 1988).
24. A. LASHIN, I. SMUROV, A. UGLOV, P. MATTEAZZI and V. TAGLIAFERRI, *Heat Tech.* **7** (2) (1989) 60.
25. I. YU. SMUROV and A. M. LASHIN, in "Physico-chemical processes in materials treatment by concentrated energy flows" (Nauka, Moscow 1989) p. 160.
26. L. PAWLOWSKI, D. LOMBARD and P. FAUCHAIS, *J. Vac. Sci. Technol.* **A3** (1985) 2494.
27. V. P. AGEEV, S. T. BURDIN and I. N. GONCHAROV, *Sci. Technol. Rev. Radiotekhnika* **31** (1983) 160.

Received 24 April
and accepted 2 August 1991